J Mater Sci (2020) 55:10339–10350

Ceramics

Enhanced microwave absorption properties of Ti_3C_2 MXene powders decorated with Ni particles

Yi Liu[1,*], Sen Zhang[1], Xiaolei Su[1], Jie Xu[1], and Yunyu Li[1,*]

[1] *Xi'an Polytechnic University, Xi'an 710048, People's Republic of China*

Received: 29 December 2019
Accepted: 23 April 2020
Published online: 5 May 2020

ABSTRACT

Double loss absorbers have attracted considerable attention due to their lightweight, thin thickness and excellent absorption performance. Herein, double loss Ti_3C_2/Ni absorbent was fabricated by decorating Ti_3C_2 MXene powders with magnetic Ni particles. Electromagnetic and microwave absorption properties of the Ti_3C_2/Ni absorbent were investigated in the frequency range of 8.2–12.4 GHz. Combining magnetic Ni particles tailored not only the electromagnetic parameters but also the microwave absorption property. The sample with Ti_3C_2/Ni powders exhibited favorable absorption performance. For the mixture with a thickness of 2.2 mm, a frequency band range of below − 10 dB reached over 8.66–11.26 GHz, with a minimum reflection loss value of − 24.3 dB at 9.8 GHz. Therefore, novel Ti_3C_2/Ni powders are expected to be a promising absorbent for thin and lightweight microwave-absorbing materials.

Introduction

Microwave absorption materials are widely used to eliminate electromagnetic radiation pollution as well as achieve radar stealth for military target. So the research of microwave absorption material is very important for both military and civilian application. In recent years, a variety of absorbents have been investigated to develop absorbers with excellent microwave absorption performance, including carbon material [1–3], semiconductor [4–6], ferrite [7–9], magnetic powders [10, 11] and their alloys [12–14]. Ever since the discovery of graphene (GP), scholars have not only set off a research boom on various types of GP composite materials, but also carried out different kinds of two-dimensional (2D) materials. Compared with traditional absorbents such as ferrite and carbon black, 2D materials have some unique advantages, including huge surface area, excellent electrical conductivity and special border effects.

As we know, graphene has been proven to own excellent properties in electromagnetic shielding and microwave absorption fields. MXene, a new 2D-layered material with a graphene-like structure, combines metal and ceramic properties with excellent electrical conductivity and special electronic properties. In addition, a large number of functional groups, interfaces and intrinsic defects on the surface make contribution to increase in dipole polarization. These properties make MXene a potential candidate for microwave absorption and electromagnetic shielding materials. The preparation and microwave

Address correspondence to E-mail: yiliu1021@163.com; liyunyu@xpu.edu.cn

https://doi.org/10.1007/s10853-020-04739-8

absorption properties of the MXene have been reported [15, 16]. Compared with the parent phase Ti_3AlC_2, Ti_3C_2's unique 2D-layered structure, high specific surface area and surface defects are beneficial to the electromagnetic wave absorption performance. However, just like graphene, the performance of individual MXene is significantly different from the expected values. So researchers combined MXene with other phases to improve its microwave absorption performance, such as MXene/ZnO [17], MXene/GP [18], MXene/$Ni_{0.5}Zn_{0.5}Fe_2O_4$ [19], MXene/CNTs [20], MXene/Fe_3O_4 [21, 22] and MXene/carbonyl iron [23], etch. And the results demonstrated the microwave absorption performances of MXene were truly enhanced by synergetic effect of the composites. But the optimization of the preparation process of MXene with excellent microwave absorption property has been continuously explored.

Composite dielectric absorbent with magnetic ones is still the main way to enhance microwave absorption properties. Both the input impedance and attenuation constant can be adjusted by the coupling effect of dielectric and magnetic loss mechanism. In this work, we prepared a novel double loss Ti_3C_2/Ni nanocomposite by a simple electroless plating process. Considering the ferromagnetic and strong saturation magnetization feature, we hope to enhance the microwave absorption performance of Ti_3C_2 with the introduction of Ni. The phase composition and microstructure of the Ti_3C_2/Ni powders were identified. The electromagnetic wave absorption properties were investigated in the frequency range of 8.2–12.4 GHz. This study makes a contribution to promoting the EM wave-absorbing property of MXenes.

Experimental procedures

Preparation of Ti_3C_2 powders

Ti_3C_2 powders were prepared by etching Ti_3AlC_2 using HF acid. The Ti_3AlC_2 powders were weighted and carefully added to 40% HF acid, and 1 g Ti_3AlC_2 is corresponding to 40 mL HF acid. Then the solution was sealed up and ultrasonic oscillated at 60 °C for 8 h. After the reaction was completed, the solution was centrifuged and the powders were washed until the supernatant is neutral. Finally, the powders were dried in an oven and the Ti_3C_2 powders were obtained.

Preparation of Ti_3C_2/Ni powders

The preparation of Ti_3C_2/Ni powders was divided into two stages: the surface pretreatment of Ti_3C_2 powders and the metallization process: firstly, weighed 10 g Ti_3C_2 and added them into an appropriate amount of absolute ethanol with mechanical stirring for 10 min at room temperature. The solution was centrifuged, separated, and the powders were rinsed with deionized water; secondly, soaked Ti_3C_2 powders to 100 mL roughening solution, stirred with a speed of 300 rpm for 30 min. After washing until the supernatant was neutral, the above powders were immersed into 500 mL (20 g/L $SnCl_2$, 40 mL/L HCl) sensitizing solution. The sensitization process lasted for 30 min accompanied with ultrasonic stirring. Finally, the sensitized Ti_3C_2 powders were removed to a 100 mL (0.1 g/L $PdCl_2$) activation solution. After 30-min reaction, the activated Ti_3C_2 powders were obtained after vacuum filtrated and washed to neutral.

In the metallization process, the pretreated Ti_3C_2 powders were immersed in an electroless plating bath. The solution was kept at 80 °C with continuous stirring at a speed of 300 rpm. Then 0.1 mol/L sodium hypophosphite solution was dropped slowly to trigger the reaction, and 0.05 mol/L NaOH solution was added to keep the pH at 10 during the plating process. After reacting for 30 min, the suspension was centrifuged, washed and dried to obtain Ti_3C_2/Ni powders. The scheme of preparation route for Ti_3C_2/Ni powders is illustrated in Fig. 1.

Characterization

The crystal structures were identified by a X-ray diffraction with a Cu Kα radiation (XPert Diffractometer, Philips, the Netherlands). The microstructure was investigated via scanning electron microscopy (Tescan China, Ltd., Shanghai, Tescan Vega3 SBH) and transmission electron microscope (JEOL JEM-F200). The electromagnetic parameters were tested using a vector network analyzer (Agilent Technologies Inc., E8362B: 10 MHz–20 GHz). The sample for electromagnetic parameter testing was prepared by mixing powders with paraffin. In a typical procedure, the weighted powders were added

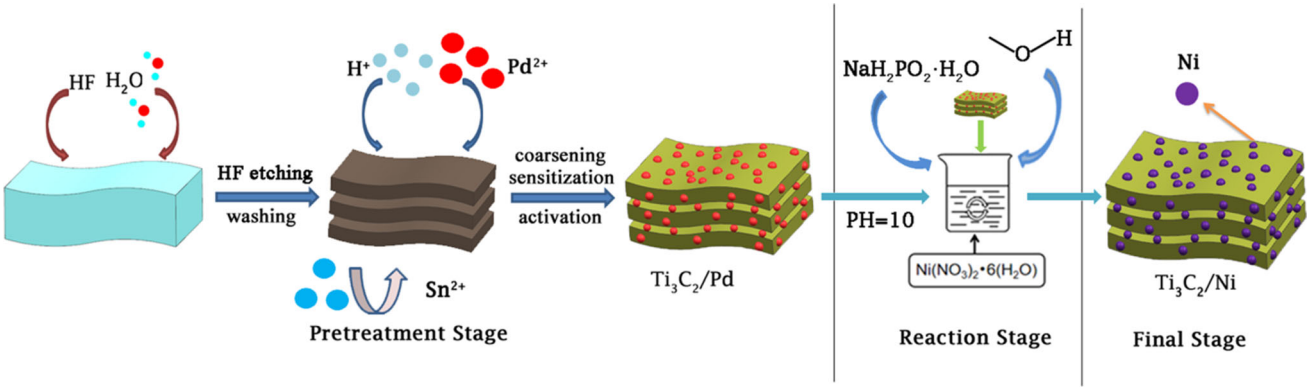

Figure 1 Scheme of preparation route for Ti_3C_2/Ni powders.

in a melt paraffin. After uniformly mixing, the mixture was pressed into a flange with a size of 22.86 mm × 10.16 mm × 2 mm. Then, the testing specimen was obtained by removing the mixture from the flange. The mass ratio of powders in the mixture was fixed 60 wt%.

Results and discussion

XRD patterns of the prepared Ni, Ti_3C_2 and Ti_3C_2/Ni powders are presented in Fig. 2. As shown in Fig. 2a, the typical peaks at 44.48°, 51.84° and 76.47° are indexed to the (111), (200) and (220) crystal planes of face-centered cubic (fcc) Ni (JCPDS#65-2865). The narrow bandwidth and sharp intensity of diffraction peaks demonstrate the Ni powders with high degree of crystallinity. In Fig. 2b, the peaks of Ti_3AlC_2 are disappeared and the typical peaks of Ti_3C_2 are indexed, indicating the Al atoms in Ti_3AlC_2 crystal lattices have been selectively etched by HF acid. Compared with the individual Ti_3C_2, the new peaks of Ni at 2θ = 44.48° and 51.84° are obviously identified, which indicates the hybrid Ti_3C_2/Ni powders are successfully prepared.

Figure 3 shows the SEM, TEM images and EDS analysis of the prepared Ni, Ti_3C_2 and Ti_3C_2/Ni powders. From Fig. 3a, the Ni particles are spherical with fine particle size, which is consistent with the XRD results. In addition, the powders aggregate together owing to the fine particle size. Figure 3b illustrates the as-prepared Ti_3C_2 possessing an accordion-like structure. The layers of Ti_3C_2 are obviously separated from each other, exhibiting an typical exfoliated morphology, which suggests the successful exfoliation of Ti_3AlC_2 after HF acid

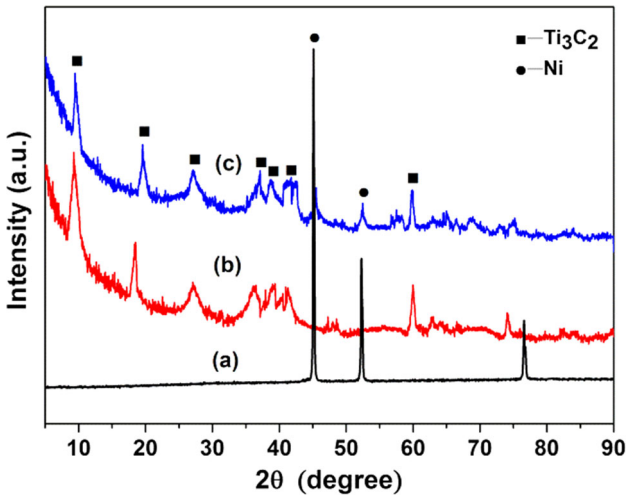

Figure 2 XRD patterns of **a** Ni; **b** Ti_3C_2; **c** Ti_3C_2/Ni powders.

etching. After electroless plating, numerous Ni nanoparticles load on the surface of Ti_3C_2 substrate is shown in Fig. 3c, d. TEM image of the Ti_3C_2/Ni powders is presented in Fig. 3e. We found that the particle size of Ni is less than 100 nm, and the Ni particles were attached on the surface of Ti_3C_2 but not in the layers, which confirms the above discussion that the nanoparticles are attached on the surface of Ti_3C_2. EDS analysis shows that the detected area exhibits strong peaks of Ti, C and Ni, as presented in Fig. 3f. It certificates that the particles coated on the surface of Ti_3SiC_2 powders are Ag.

The frequency dependence of complex permittivity and permeability for the prepared Ni, Ti_3C_2 and Ti_3C_2/Ni powders is presented in Fig. 4. The real part of complex permittivity (ε') and permeability (μ') represents the storage ability of electromagnetic energy, while the imaginary part (ε'' and μ'') is related to the dissipating capacity [24]. It can be seen that the

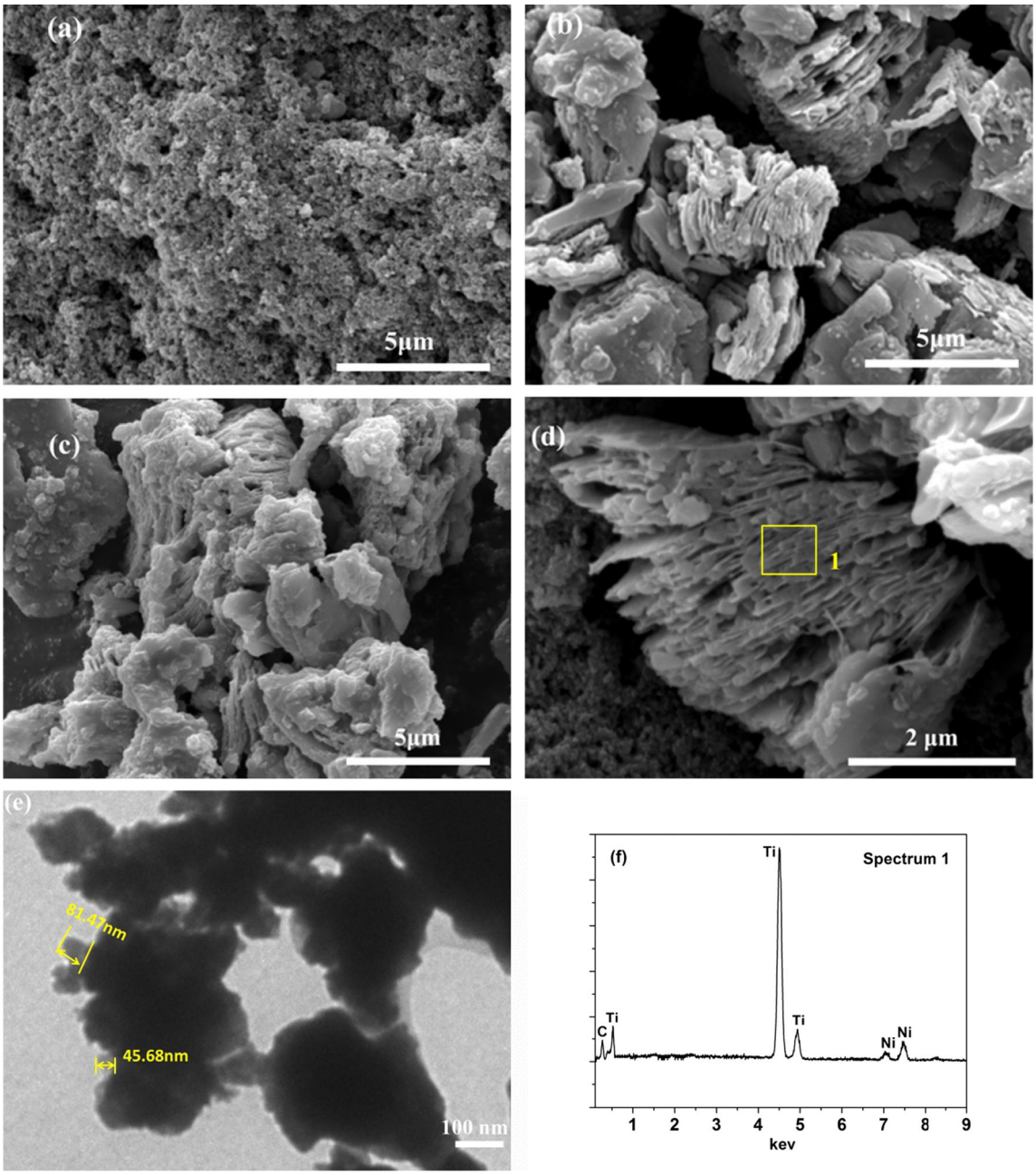

Figure 3 SEM, TEM images and EDS analysis of powders: **a** Ni; **b** Ti_3C_2; **c** Ti_3C_2/Ni; **d** magnification of Ti_3C_2/Ni; **e** TEM image of Ti_3C_2/Ni; **f** spectrum of zone 1.

values of ε' and ε'' for hybrid Ti_3C_2/Ni powders are much larger than that of individual Ti_3C_2 and Ni powders, and the real and imaginary part value of Ni powders is the lowest. The complex permittivity of Ni almost stays independent with the frequency, which is about 9.0 and 1.2 for the real and imaginary part, respectively. The dielectric loss, which is defined as $\tan\delta = \varepsilon''/\varepsilon'$, reflecting the contribution of polarization loss mechanism for electromagnetic dissipation ability. The low complex permittivity of Ni that may be ascribed to it is a magnetic particle, and polarization loss is not the main dissipating mechanism. The ε', ε'' and $\tan\delta$ of Ti_3C_2 are higher than those of Ni. It is ascribed that the Ti_3C_2 is a typical dielectric loss absorbent and its large specific surface area and multiple dangling bonds are beneficial to increase the dielectric loss. For the hybrid Ti_3C_2/Ni powders, both the complex permittivity

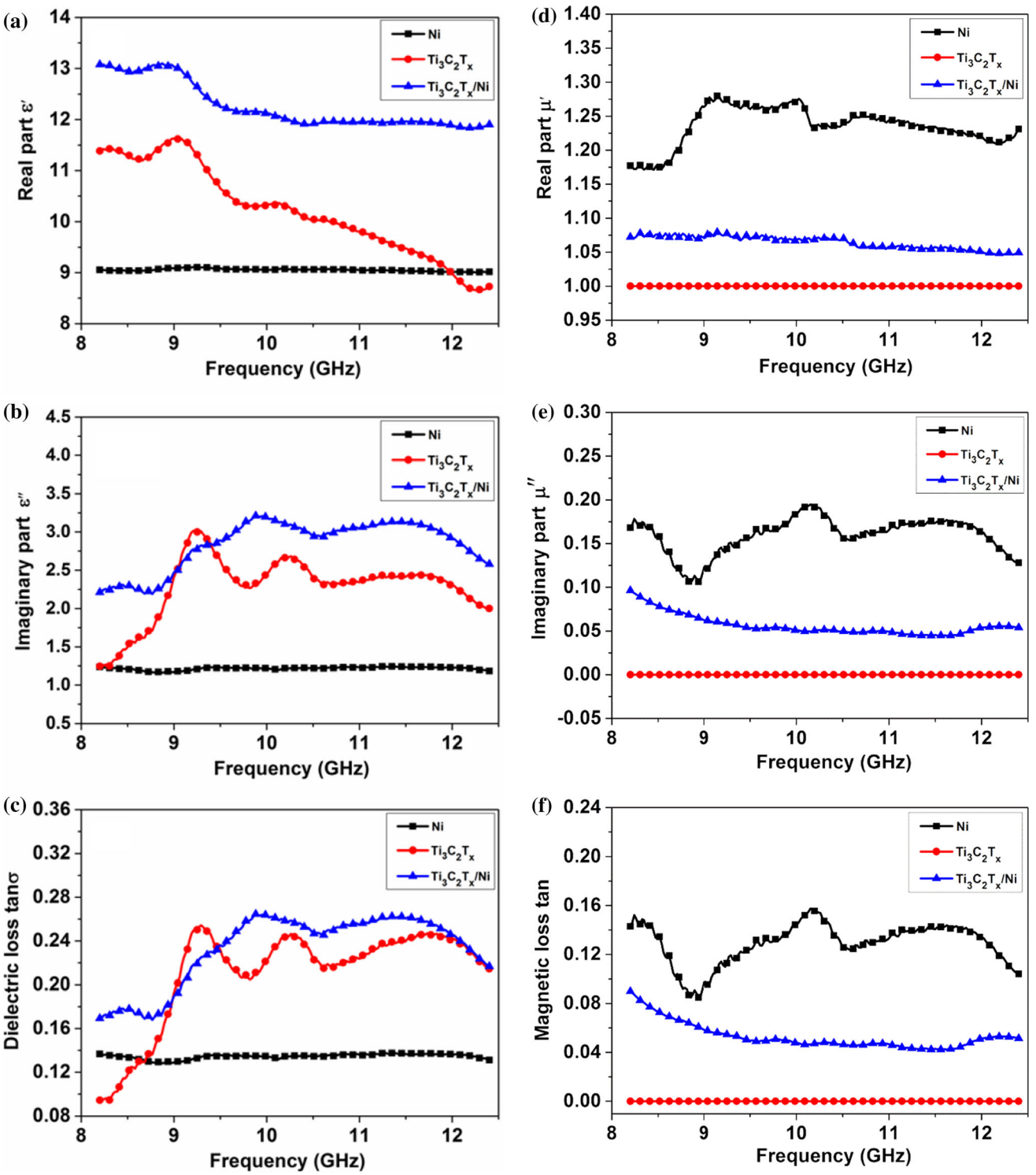

Figure 4 Frequency dependence of electromagnetic parameters for powders: **a** real part of complex permittivity; **b** imaginary part of complex permittivity; **c** dielectric loss; **d** real part of complex permeability; **e** imaginary part of complex permeability; **f** magnetic loss.

and dielectric loss are enhanced. The real part increases to 13.1–11.9 and the imaginary part reaches to 2.2–2.6 in the frequency range of 8.2–12.4 GHz. Polarization effects determine the real part of complex permittivity and include interfacial and relaxation polarization. After compositing Ni with Ti_3C_2, a

numerous of interfaces form between the Ni and Ti_3C_2 particles. What's more, the introduction of Ni/paraffin interface also augments the quantity of interfaces. So the increases of interfaces enhance the interfacial and relaxation polarization effect, which is beneficial to the higher ε' of Ti_3C_2/Ni.

Different from the real part of complex permittivity, imaginary part is not only affected by polarization effect, but also influenced by electric conductivity. According to the Debye theory, the imaginary part can be illustrated as $\varepsilon'' = \varepsilon'_{relax} + \sigma/2\pi\varepsilon_0 f$ [25, 26], where ε'_{relax} is the relaxation polarization loss, σ is the electrical conductivity, f is frequency of electromagnetic wave, and ε_0 is the dielectric constant of free space. As discussed above, the polarization effect is enhanced for the hybrid Ti_3C_2/Ni powders after compositing Ti_3C_2 with Ni. It not only enhances the real part, but also helps to improve the imaginary part. In addition, the electrical conductivity of Ni is much higher than that of Ti_3C_2. So the introduction of Ni should improve the electric conductivity of Ti_3C_2/Ni powders compared with the individual Ti_3C_2, which also makes contribution to the improvement of imaginary part.

The complex permeability $(\mu' - j\mu'')$ of the powders is shown in Fig. 4d–f. It is observed that the value of Ti_3C_2 is $1 - 0j$, which indicates Ti_3C_2 is a nonmagnetic material and dielectric loss is the main dissipating mechanism. Ni is a typical magnetic material with strong saturation magnetization. In this case, the real part of complex permeability is 1.18–1.23 and the imaginary part is 0.17–0.13 after the Ni powders are mixed with paraffin. The higher tanδ value (0.14–0.1) demonstrates the magnetic loss is the dissipating mechanism. After the Ni is composited with MoS_2, both the μ' and μ'' of Ti_3C_2/Ni powders are enhanced compared with bare Ti_3C_2. As discussed above, the Ti_3C_2 is a typical dielectric loss absorbent, while Ni is a magnetic loss absorbent. So the replacement of Ti_3C_2 by Ni can certainly improve the complex permeability of Ti_3C_2 powders. In addition, we can conclude that the electromagnetic parameters can be adjusted by combining Ti_3C_2 with Ni powders.

Generally, the dielectric loss mechanism can be analyzed by the Cole–Cole curve. The above discussion has illustrated the dielectric loss mainly depends on dipolar relaxation polarization, interfacial polarization and conductance loss. According to the Debye theory, the relationship between the real and imaginary part of complex permittivity is expressed as follows [27–29]: $\left(\varepsilon' - \frac{\varepsilon_s - \varepsilon_\infty}{2}\right)^2 + (\varepsilon'')^2 = \left(\frac{\varepsilon_s - \varepsilon_\infty}{2}\right)^2$. So the Cole–Cole curve should be a semicircle if only dipolar relaxation polarization contributes to the dielectric loss. And it will deviate from the regular circle if there are multiple loss effects. As can be seen from Fig. 5a, the Cole–Cole curve of individual Ni is close to a circle, indicating the polarization effect is sole, while the Cole–Cole curve of Ti_3C_2 consists of several semicircles, as presented in Fig. 5b. The main reason is that large specific surface area and multiple dangling bonds after etching by HF acid introduce different polarization effects. After combining Ti_3C_2 with Ni, not only the interfacial polarization effect between Ti_3C_2 and Ni is added, but also the conduction loss mechanism is introduced which mainly results in the irregular Cole–Cole curve of Ti_3C_2/Ni, as shown in Fig. 5c.

The magnetic loss mechanism is further discussed. The eddy current coefficient, which is expressed as $C_0 = \mu''(\mu')^{-2}f^{-1}$, can be explained by the magnetic dissipating mechanism. In theory, the loss effect to dissipate electromagnetic wave consists of domain wall resonance, hysteresis loss, eddy current resonance and natural resonance [30]. However, in this weak electromagnetic field (8.2–12.4 GHz), the hysteresis loss could be excluded [31]. What's more, the domain wall resonance only makes influence on the properties at megahertz frequency range [32]. So it can be concluded that the natural resonance and eddy current resonance mainly contribute to the magnetic loss. If C_0 is a constant, the eddy current loss should be the individual dissipating mechanism. However, it can be seen from Fig. 6 that both the C_0 of Ni and Ti_3C_2/Ni powders decreases with the increasing frequency. So both the eddy current and natural resonance loss make the contribution to the magnetic loss.

Microwave absorption properties of the powders are also investigated. Reflection loss (RL) is used to evaluate the absorption performance of microwave absorption material, which can be illustrated as follows according to the transmission line theory [33–35]:

$$\mathrm{RL\,(dB)} = 20\log\left|{(Z_{in} - Z_0)}/{(Z_{in} + Z_0)}\right| \quad (1)$$

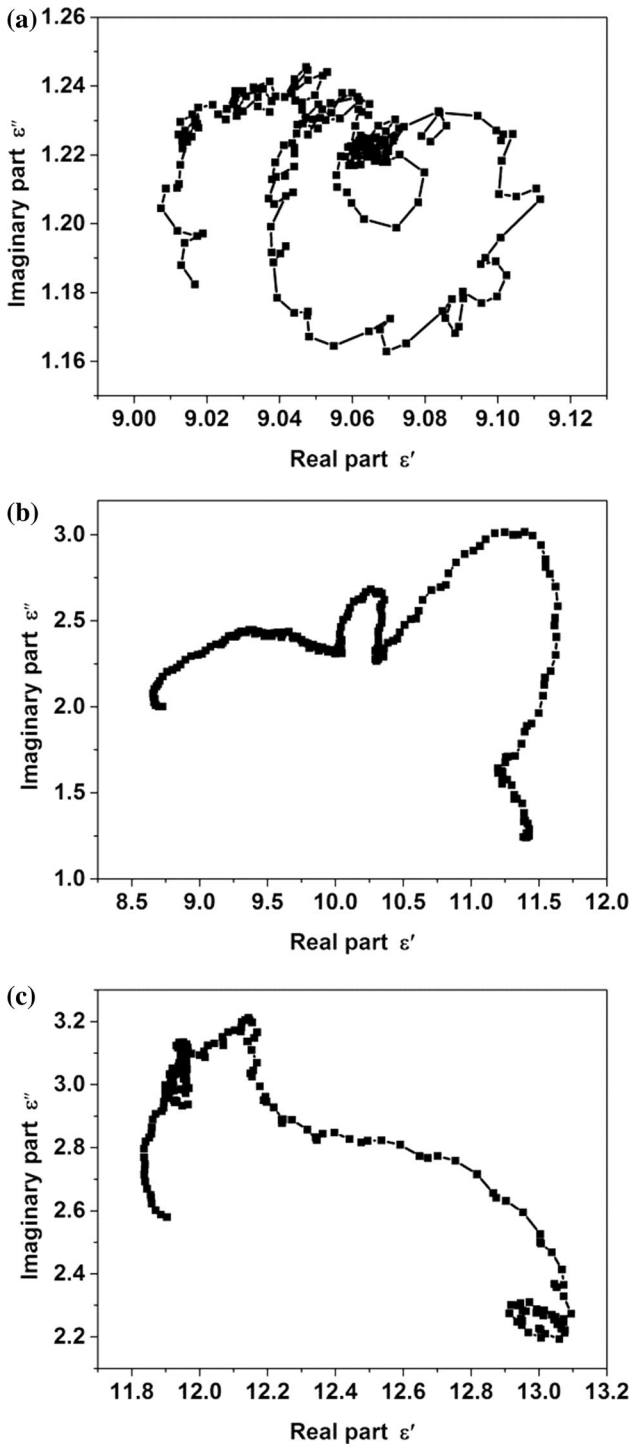

Figure 5 Cole–Cole curves of **a** Ni, **b** Ti_3C_2 and **c** Ti_3C_2/Ni powders.

$$Z_0 = \sqrt{\frac{\mu_0}{\varepsilon_0}} \tag{2}$$

$$Z_{in} = Z_0 \sqrt{\mu_r/\varepsilon_r} \tanh\left[j\frac{2\pi}{c}\sqrt{\mu_r\varepsilon_r}fd\right] \tag{3}$$

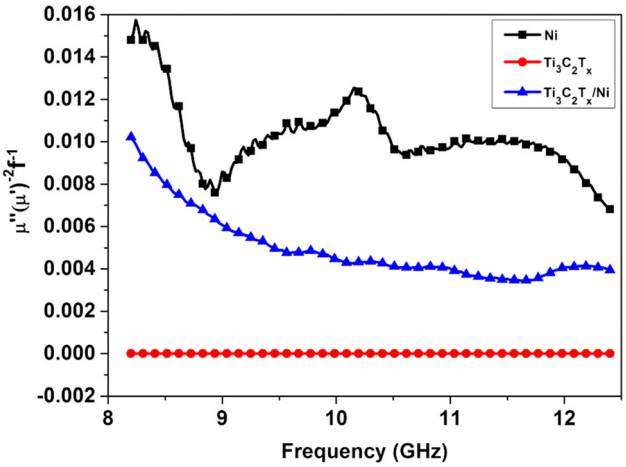

Figure 6 $\mu''(\mu')^{-2}f^{-1}$ values of powders in frequency range of 8.2–12.4 GHz.

where Z_0 and Z_{in} are the input impedances of free space and microwave-absorbing material, respectively. ε_r is the relative complex permittivity, and μ_r is the relative complex permeability. f is the frequency of electromagnetic wave, d is the thickness of absorber, and c is the velocity of light. Figure 7 shows the RL values of the samples containing Ni, Ti_3C_2 and Ti_3C_2/Ni powders with different thicknesses in the frequency range of 8.2–12.4 GHz. 3D color mapping displays the relationship between the reflection loss, frequency and thickness. It can be seen from Fig. 7a that the Ni powders display a weak reflection loss, and the RL values for the samples with all thicknesses are above − 15 dB. The poor microwave absorption property may be owing to its low complex permittivity and dielectric loss, while the reflection loss value of Ti_3C_2 is a little lower than Ni powders (above − 20 dB), which indicates Ti_3C_2 owning a better microwave absorption performance. As discussed above, the large specific surface area and multiple dangling bonds help to increase the dielectric loss. Although the magnetic loss makes no contribution to absorption property, the higher dielectric loss dominates and results in a better absorbing performance. After Ti_3C_2 is composited with Ni, the RL value further decreases and the absorption performance of Ti_3C_2/Ni powders is enhanced. As shown in Fig. 3, the Ni particles are attached on Ti_3C_2 powders, which inevitably increases the interface polarization effect and dielectric loss. What's more, the introduction of magnetic Ni also helps to improve the magnetic loss because Ti_3C_2 is nonmagnetic

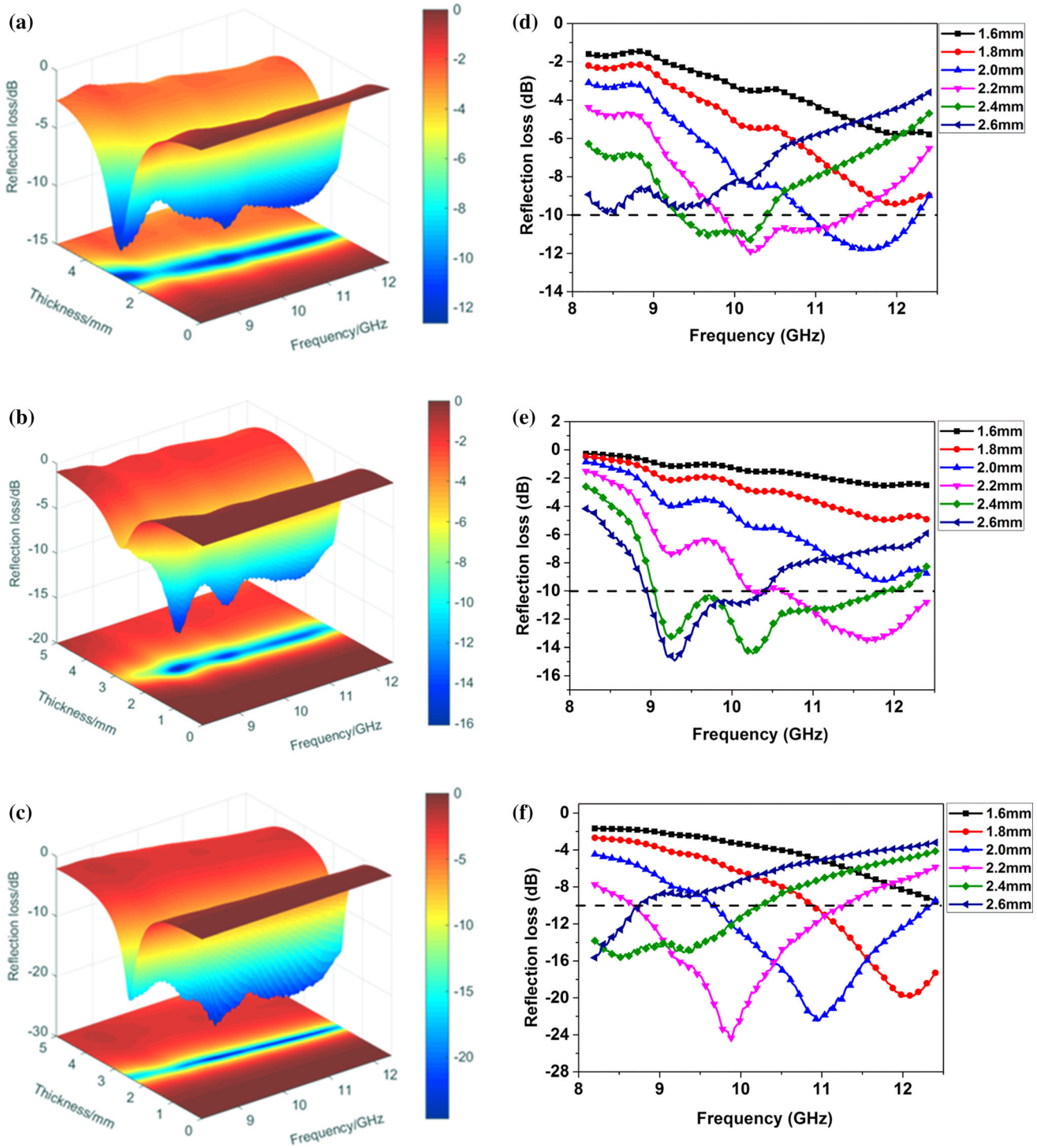

Figure 7 Microwave absorption performances of **a**, **d** Ni, **b**, **e** Ti_3C_2 and **c**, **f** Ti_3C_2/Ni.

material. The synergistic loss mechanism of magnetic and dielectric loss contributes to dissipating electromagnetic energy. So it can be concluded that the double loss effect is more beneficial to dissipate electromagnetic wave than single dielectric loss or magnetic loss.

To clarify the microwave absorption performance clearly, we analyze the RL values of the samples with thicknesses of 1.6–2.6 mm, as shown in Fig. 7d–f. The

RL values of the samples are affected by the thickness of the samples. As the thickness increases from 1.6 to 2.6 mm, the RL value decreases initially but increases in the frequency range of 8.2–12.4 GHz. For the sample containing Ni with a thickness of 2.2 mm, a minimum RL value of − 12 dB at 10.24 GHz is obtained and the effective absorption bandwidth (EAB, RL < − 10 dB) is in the frequency range of 9.84–11.46 GHz. The EAB of the sample containing individual Ti_3C_2 is much broader than Ni. And the bandwidth reaches to 2.94 GHz in the frequency range from 9 to 11.94 GHz for the sample with a thickness of 2.4 mm. However, the lowest RL value is achieved after compositing Ti_3C_2 with Ni powders. As for the Ti_3C_2/Ni/paraffin mixture, the minimum RL value reaches to the lowest − 24.3 dB at 9.8 GHz for the sample with a thickness of 2.2 mm. Although the EAB (8.66–11.26 GHz) is narrower than the individual Ti_3C_2, the thickness of the sample is thinner. In addition, the mixture with a thickness of 2.0 mm also has an EAB in the frequency range of 9.67–12.34 GHz. It indicates that the microwave absorption performance of Ti_3C_2/Ni/paraffin owns favorable absorption performance with wider range of thickness. Also, the microwave absorption performance can be adjusted by changing the sample thickness.

In order to achieve high efficiency absorption performance, electromagnetic wave must enter the absorber and be attenuated. So two key factors should be satisfied. One is impedance matching condition, and the other is electromagnetic wave dissipating capacity. The former one dominates the amount of electromagnetic wave entering into the material directly, which requires the impedance of absorber is approaching to that of the free space. And the latter one determines the loss amount of electromagnetic wave in the internal material, which should be as large as possible. Figure 8 shows the input impedance of the paraffin mixture containing Ni, Ti_3C_2 and Ti_3C_2/Ni powders. The value of 377 Ω is designated as the free space impedance. The input impedance of Ni lays in the range of 349–340 Ω, deviating from the free space impedance, while the impedance of Ti_3C_2 is lower than that of Ni, which is little closer to the free space impedance. Such phenomenon indicates Ni and Ti_3C_2. Both exhibit poor impedance matching condition. Comparatively, the Ti_3C_2/Ni presents relatively smaller input impedance value which is closer to 377 Ω, so the reflection of electromagnetic wave is less at the air-microwave absorption material interface.

Attenuation constant (α) of absorber can be expressed as [36–38]:

$$\alpha = \frac{\sqrt{2}\pi f}{c}\sqrt{\mu''\varepsilon'' - \mu'\varepsilon' + \sqrt{(\mu'^2 + \mu''^2)(\varepsilon'^2 + \varepsilon''^2)}} \quad (4)$$

Figure 9 shows the attenuation constant of paraffin with Ni, Ti_3C_2 and Ti_3C_2/Ni powders. It is observed that the α increases with the rising frequency, which indicates the samples exhibit strong dissipating ability in higher-frequency region. Although the attenuation constant (α) value of Ni (78.3–101.7 Np/m) is larger than that of Ti_3C_2 (31.6–87.4 Np/m), the absorption performance is worse. It is mainly attributed to the deviation of impedance matching condition results in stronger reflection. This phenomenon indicates that high attenuation constant α is not equal to the strong dissipating capacity. The attenuation constant value of Ti_3C_2/Ni powders is 88.1–130.2 Np/m, which is the highest among the powders. Figure 10 shows the schematic diagram of microwave absorption mechanism for Ti_3C_2/Ni powders. Combining the best impedance matching condition, the Ti_3C_2/Ni powders exhibit the most favorable microwave absorption performance.

Conclusion

In this work, we develop a new way to improve the microwave absorption property of Ti_3C_2. A novel composite of Ti_3C_2/Ni powders has been prepared by a typical electroless plating method. Compared

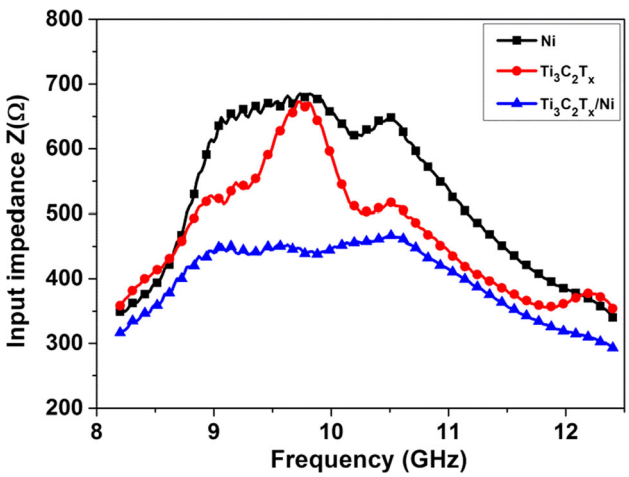

Figure 8 Input impedance of Ni, Ti_3C_2 and Ti_3C_2/Ni powders.

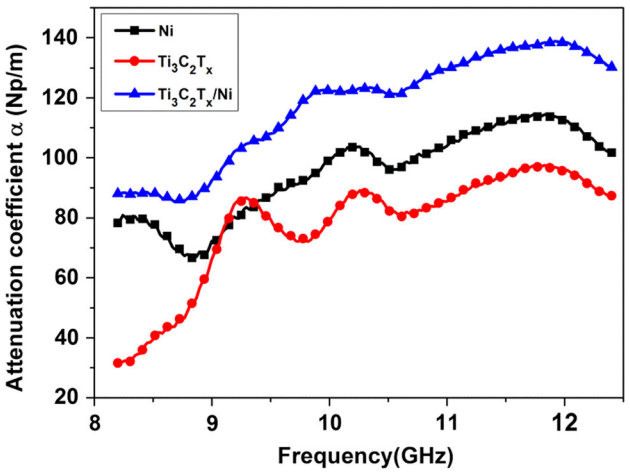

Figure 9 Attenuation constants of Ni, Ti_3C_2 and Ti_3C_2/Ni powders.

with the individual Ti_3C_2 and Ni powders, the hybrid Ti_3C_2/Ni powders exhibit the most favorable microwave absorption performance with a minimum reflection loss (RL) value of − 24.3 dB at 9.8 GHz. Both the impedance matching condition and dissipating ability of Ti_3C_2/Ni powders can be tuned by compositing with Ni. This work puts forward a new way to enhance the electromagnetic wave-absorbing property of MXenes.

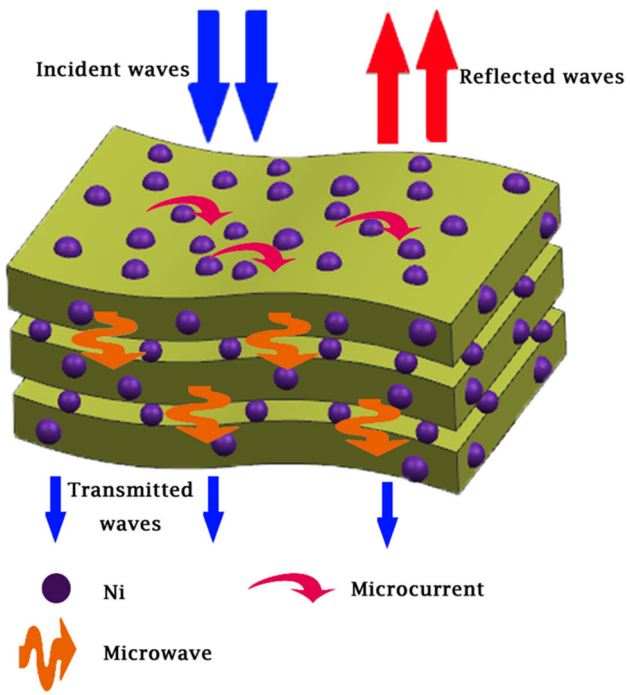

Figure 10 Scheme of microwave dissipating mechanism for Ti_3C_2/Ni powders.

Acknowledgements

This study was funded by Natural Science Basis Research Plan in Shaanxi Province of China (No. 2019JQ-853), PHD Start-up Fund of XPU (BS1615), the Young Talent Fund of University Association for Science and Technology in Shaanxi, China (No. 20170521), Scientific Research Program Funded by Shaanxi Provincial Education Department (Program No. 18JK0353), Scientific and Technological Plan Project of Xi'an Science and Technology Bureau (2019217114GXRC007CG008-GXYD7.6, 201805030YD 8CG14(14)), Science and Technology Guiding Project of China Textile Industry Association (No. 2019045), Shaanxi Special Talents Support Plan, Shaanxi University Youth Outstanding Talents Support Plan and National Natural Science Foundation of China (No. 51802244).

Compliance with ethical standards

Conflict of interest There are no conflicts of interest.

References

[1] Wei H, Yin X, Li X, Li M, Dang X, Zhang L, Cheng L (2019) Controllable synthesis of defective carbon nanotubes/$Sc_2Si_2O_7$ ceramic with adjustable dielectric properties for broadband high-performance microwave absorption. Carbon 147:276–283

[2] Kumar R, Choudhary HK, Pawar SP, Bose S, Sahoo B (2017) Carbon encapsulated nanoscale iron/iron-carbide/graphite particles for EMI shielding and microwave absorption. Phys Chem Chem Phys 19:23268–23279

[3] Choudhary HK, Sahoo B, Pawar SP, Bose S (2017) Microwave absorption property of hydrothermal synthesized RGO/$PbFe_{12}O_{19}$ nanocomposite. Asian J Converg Technol (AJCT) 3:918–923

[4] Huang X, Zhang M, Qin Y, Chen Y (2019) Bead-like Co-doped ZnO with improved microwave absorption properties. Ceram Int 45:7789–7796

[5] Ur Rehman S, Liu J, Ahmed R, Bi H (2019) Synthesis of composite of ZnO spheres with polyaniline and their microwave absorption properties. J Saudi Chem Soc 23:385–391

[6] Kuang J, Jiang P, Hou X, Xiao T, Zheng Q, Wang Q, Liu W, Cao W (2019) Dielectric permittivity and microwave absorption properties of SiC nanowires with different lengths. Solid State Sci 91:73–76

[7] Choudhary HK, Pawar SP, Kumar R, Anupama AV, Bose S, Sahoo B (2017) Mechanistic insight into the critical concentration of barium hexaferrite and the conductive polymeric phase with respect to synergistically electromagnetic interference (EMI) shielding. ChemistrySelect 2:830–841

[8] Choudhary HK, Pawar SP, Bose S, Sahoo B (2018) EMI shielding performance of lead hexaferrite/polyaniline composite in 8–18 GHz frequency range. AIP Conf Proc 1953:120061–120069

[9] Choudhary HK, Kumar R, Pawar SP, Bose S, Sahoo B (2020) Effect of microstructure and magnetic properties of Ba-Pb-hexaferrite particles on EMI shielding behavior of Ba-Pb-hexaferrite-polyaniline-wax nanocomposites. J Electron Mater 49:1618–1629

[10] Choudhary HK, Kumar R, Pawar SP, Sundararaj U, Sahoo B (2019) Enhancing absorption dominated microwave shielding in Co@C-PVDF nanocomposites through improved magnetization and graphitization of the Co@C-nanoparticles. Phys Chem Chem Phys 21:15595–15608

[11] Kumar R, Choudhary HK, Anupama AV, Menon AV, Pawar SP, Bose S, Sahoo B (2019) Nitrogen doping as a fundamental way to enhance the EMI shielding behavior of cobalt particle-embedded carbonaceous nanostructures. New J Chem 43:5568–5580

[12] Wang L, Xiong H, Rehman SU, Tan Q, Chen Y, Zhang L, Yang J, Wu F, Zhong M, Zhong Z (2019) Microwave absorbing property enhancement of FeSiCr nanomaterials by regulating nanoparticle size. J Alloys Compd 803:631–636

[13] He Y, Pan S, Cheng L, Luo J, Yu J (2019) Improving microwave absorbing property of flaky Ce_2Co_{17} alloys by Ni content and carbonyl iron powder. J Electron Mater 48:1574–1581

[14] Choudhary HK, Kumar R, Pawar SP, Anupama AV, Bose S, Sahoo B (2018) Effect of coral-shaped yttrium iron garnet particles on the EMI shielding behaviour of yttrium iron garnet-polyaniline-wax composites. ChemistrySelect 3:2120–2130

[15] Qing Y, Zhou W, Luo F, Zhu D (2016) Titanium carbide (MXene) nanosheets as promising microwave absorbers. Ceram Int 42:16412–16416

[16] Han M, Yin X, Wu H, Hou Z, Song C, Li X, Zhang L, Cheng L (2016) Ti_3C_2 MXenes with modified surface for high-performance electromagnetic absorption and shielding in the X-band. ACS Appl Mater Interfaces 8:21011–21019

[17] Qian Y, Wei H, Dong J, Du Y, Fang X, Zheng W, Sun Y, Jiang Z (2017) Fabrication of urchin-like ZnO-MXene nanocomposites for high-performance electromagnetic absorption. Ceram Int 43:10757–10762

[18] Qing Y, Nan H, Luo F, Zhou W (2017) Nitrogen-doped graphene and titanium carbide nanosheet synergistically reinforced epoxy composites as high-performance microwave absorbers. RSC Adv 7:27755–27761

[19] Li Y, Zhou X, Wang J, Deng Q, Li M, Du S, Han YH, Lee J, Huang Q (2017) Facile preparation of in situ coated $Ti_3C_2T_x$/$Ni_{0.5}Zn_{0.5}Fe_2O_4$ composites and their electromagnetic performance. RSC Adv 7:24698–24708

[20] Li X, Yin X, Han M, Song C, Xu H, Hou Z, Zhang L, Cheng L (2017) Ti_3C_2 MXenes modified with in situ grown carbon nanotubes for enhanced electromagnetic wave absorption properties. J Mater Chem C 5:4068–4074

[21] Liu P, Yao Z, Ng VMH, Zhou J, Kong LB, Yue K (2018) Facile synthesis of ultrasmall Fe_3O_4 nanoparticles on MXenes for high microwave absorption performance. Compos A Appl Sci Manuf 115:371–382

[22] Liu P, Ng VMH, Yao Z, Zhou J, Kong LB (2018) Ultrasmall Fe_3O_4 nanoparticles on MXenes with high microwave absorption performance. Mater Lett 229:286–289

[23] Yan S, Cao C, He J, He L, Qu Z (2019) Investigation on the electromagnetic and broadband microwave absorption properties of Ti_3C_2 Mxene/flaky carbonyl iron composites. J Mater Sci Mater Electron 30:6537–6543

[24] Zhou W, Hu X, Bai X, Zhou S, Sun C, Yan J, Chen P (2011) Synthesis and electromagnetic, microwave absorbing properties of core–shell Fe_3O_4-poly(3, 4-ethylenedioxythiophene) microspheres. ACS Appl Mater Interfaces 3:3839–3845

[25] Li J, Feng W, Wang J, Zhao X, Zheng W, Yang H (2015) Impact of silica-coating on the microwave absorption properties of carbonyl iron powder. J Magn Magn Mater 393:82–87

[26] Liu Y, Li Y, Luo F, Su X, Xu J, Wang J, Qu Y, Shi Y (2017) Mechanical, dielectric and microwave absorption properties of TiC/cordierite composite ceramics. J Mater Sci Mater Electron 28:12115–12121

[27] Sun X, He J, Li G, Tang J, Wang T, Guo Y, Xue H (2013) Laminated magnetic graphene with enhanced electromagnetic wave absorption properties. J Mater Chem C 1:765–777

[28] Xing W, Li P, Wang H, Lei Q, Huang Y, Fan J, Xu G (2018) The similar Cole–Cole semicircles and microwave absorption of hexagonal Co/C composites. J Alloys Compd 750:917–926

[29] Peng J, Peng Z, Wang L, Zheng L, Zhu Z, Li G, Jiang T (2019) Microwave-assisted one-step synthesis of FeCo/-graphene nanocomposite for microwave absorption. Springer, Cham, pp 329–340

[30] Wu Q, Wu G, Wang L, Hu W, Wu H (2015) Facile synthesis and optical properties of Prussian Blue microcubes and hollow Fe_2O_3 microboxes. Mater Sci Semicond Process 30:476–481

[31] Li Z, Deng Y, Shen B, Hu W (2009) Preparation and microwave absorption properties of Ni–Fe_3O_4 hollow spheres. Mater Sci Eng B 164:112–115

[32] Du Y, Liu W, Qiang R, Wang Y, Han X, Ma J, Xu P (2014) Shell thickness-dependent microwave absorption of core–shell Fe_3O_4@C composites. ACS Appl Mater Interfaces 6:12997–13006

[33] Qiang C, Xu J, Zhang Z, Tian L, Xiao S, Liu Y, Xu P (2010) Magnetic properties and microwave absorption properties of carbon fibers coated by Fe_3O_4 nanoparticles. J Alloys Compd 506:93–97

[34] Zhang L, Zhu H (2009) Dielectric, magnetic, and microwave absorbing properties of multi-walled carbon nanotubes filled with Sm_2O_3 nanoparticles. Mater Lett 63:272–274

[35] Wu H, Wang L, Guo S, Shen Z (2012) Double-layer structural design of dielectric ordered mesoporous carbon/paraffin composites for microwave absorption. Appl Phys A 108:439–446

[36] Dan C, Liu X, Yu R, Ye J, Shi Y (2016) Enhanced microwave absorption properties of flake-shaped FePCB metallic glass/graphene composites. Compos A Appl Sci Manuf 89:33–39

[37] Lv H, Ji G, Zhang H, Li M, Zuo Z, Zhao Y, Zhang B, Tang D, Du Y (2015) Co_xFe_y@C composites with tunable atomic ratios for excellent electromagnetic absorption properties. Sci Rep 5:18249–18259

[38] Qiao M, Lei X, Ma Y, Tian L, Su K, Zhang Q (2016) Dependency of tunable microwave absorption performance on morphology-controlled hierarchical shells for core-shell Fe_3O_4@MnO_2 composite microspheres. Chem Eng J 304:552–562